Journal of Structural Geology 33 (2011) 1639–1649

Contents lists available at SciVerse ScienceDirect

Journal of Structural Geology

journal homepage: www.elsevier.com/locate/jsg

Formation of chocolate-tablet boudins in a foreland fold and thrust belt: A case study from the external Variscides (Almograve, Portugal)

G. Zulauf[a,*], G. Gutiérrez-Alonso[b], R. Kraus[c], R. Petschick[a], S. Potel[d]

[a] Institut für Geowissenschaften, Universität Frankfurt a.M., Altenhöferallee 1, D-60438 Frankfurt am Main, Germany
[b] Departamento de Geología, Universidad de Salamanca, 37008 Salamanca, Spain
[c] Universita degli Studi di Genova, Dipartimento per lo studio del territorio e delle sue risorse (Dip.Te.Ris.), Viale Benedetto XV, 5 Genova 16132, Italy
[d] Enseignant-Chercheur, Minéralogie, Pétrologie, Institut Polytechnique LaSalle Beauvais, 19 rue Pierre Waguet, BP 30313, F-60026 BEAUVAIS Cedex, France

ARTICLE INFO

Article history:
Received 2 November 2010
Received in revised form
24 August 2011
Accepted 26 August 2011
Available online 5 September 2011

Keywords:
Chocolate-tablet boudins
Extension fracture boudinage
External Variscides

ABSTRACT

Chocolate-tablet boudins of quartzite are restricted to steep limbs of D_1-folds along the SW coast of Portugal. The chocolate-tablet geometry results from older vertical and younger horizontal quartz veins. Both sets of veins developed during similar conditions by extension fracture in pre-existing necked domains: (1) both veins show stretched crystal fibers; (2) the boudin aspect ratio is the same in vertical (3.0 ± 1.4) and in horizontal sections (2.9 ± 1.2); (3) temperatures obtained from fluid inclusions are similar ($200 \pm 20°$ for vertical and 230 ± 22 °C for horizontal veins) and are compatible with temperatures obtained from illite crystallinity (ca. 200–ca. 250 °C). Given thermal equilibrium between the host rock and the precipitating fluid, the chocolate-tablet boudins formed close to the metamorphic peak. We interpret that the vertical veins developed after the limbs of the D_1-folds had attained their steep attitude and the orientation of the greatest and intermediate principal strain axes had interchanged. Subsequently, the initial strain field was restored and opening of horizontal veins led to the chocolate-tablet geometry. The direction of the main shortening direction was constant from the initial buckling stage via isoclinal folding and during all boudinage stages.

1. Introduction

Boudinage is a process where a competent layer embedded in an incompetent material is segmented as a result of stretching parallel to the layer. The name *boudin* was first used by Lohest (1909) to describe structures in metamorphosed Devonian sediments of the Ardennes, Belgium, although they were re-interpreted recently as structures unrelated to boudinage (Kenis et al., 2002). These structures are barrel-shaped in profile and each barrel is separated from the next by a vein. In three dimensions, they appear as large flattened cylinders or "sausages" (boudins) lying side by side. The geometry of boudins is one of a complete spectrum of geometries from isolated rectangular blocks (*torn boudins* of Goscombe et al., 2003) to a regular thickening and thinning of the competent layer known as pinch-and-swell structure (*drawn boudins* of Goscombe et al., 2003). This spectrum results from a range of rheological behavior of the competent layer from brittle, when tensile fracture occurs, to ductile, when 'failure' occurs by localized necking.

Most boudins described in the literature show a cylindrical geometry. Wegmann (1932) found non-cylindrical boudinage where two perpendicular sets of boudin necks occur. He termed such boudins with rectangular plan-view *chocolate-tablet structure*. Similar structures are described from natural rocks deformed in various conditions for different tectonic settings (Ramberg, 1955; Coe, 1959; Fyson, 1962; Ramsay, 1967; Schwerdtner and Clark, 1967; Crespo-Blanc, 1995; Casey et al., 1983; Ormand and Czeck, 2003; Albertz and Paterson, 2002; Witkowski and Crespi, 2002; Tricart et al., 2004). Chocolate-tablet boudins are common in individual competent sedimentary layers and are often exceedingly well formed in competent pyrite-rich layers of diagenetic origin contained in incompetent sediments (Casey et al., 1983; Ramsay and Huber, 1983: Figs. 13.29 and 13.30).

The formation of chocolate-tablet boudins is still a matter of debate. Chocolate-tablet boudinage is generally assumed to be characteristic for oblate deformations where the principal shortening axis, *Z*, is perpendicular to the boudinaged layer (Weijermars, 1997, p. 250; Zulauf et al., 2003). If this assumption is true, chocolate-tablet boudins should frequently occur in rheologically anisotropic rocks, because flattening deformations are common (Pfiffner and Ramsay, 1982). However, if the boudins arise *during a single oblate deformation*, their necks should be generally rather

* Corresponding author.
E-mail addresses: g.zulauf@em.uni-frankfurt.de (G. Zulauf), sebastien.potel@lasalle-beauvais.fr (S. Potel).

0191-8141/$ – see front matter © 2011 Elsevier Ltd. All rights reserved.
doi:10.1016/j.jsg.2011.08.009

irregular, or mostly radial, although they might occur more frequently and show a wider separation where they are subperpendicular to the maximum extension direction (Ramsay and Huber, 1983). This predicted irregular geometry was confirmed experimentally by Ghosh (1988), Zulauf (2004), and Zulauf et al., (2010), who found that boudinage for a flattening bulk strain with equal layer-parallel extension in all directions leads to the development of roundish or polygonal boudins in plan-view.

Chocolate-tablet boudins, on the other hand, should develop as a result of *polyphase deformation* or could be controlled by a *mechanical anisotropy in lineated rocks* (Ramsay and Huber, 1983, p. 65; Ghosh, 1988; Reber et al., 2010). In the present study, we examine well exposed chocolate-tablet boudins that formed in Carboniferous siliciclastics along the SW coast of Portugal (Marques et al., 2010; Reber et al., 2010). The exposures are located close to the village Almograve (Fig. 1). The rocks are syn-orogenic Late Visean to early Late Namurian slate and intercalated quartzite in a S-vergent foreland fold and thrust belt of the South Portuguese Zone (Fig. 1) within the Variscan belt of western Europe (Brejeira Formation, Oliveira, 1990; Quesada, 1991). The tectonic evolution of this region is described in numerous recent papers (e.g. Silva et al., 1990; Soriano y Casas, 2002; Onezime et al., 2002, 2003 and Marques et al., 2010). Pressure-temperature conditions ranged from diagenetic to the lower anchizone (Abad et al., 2001). S-vergent folds and thrusts formed during the Mississippian as a result of independent particulate flow of the not fully lithified turbiditic sediments (Marques et al., 2010). Subsequent NNE-trending dextral strike-slip faults formed late during the major folding event (Marques et al., 2002).

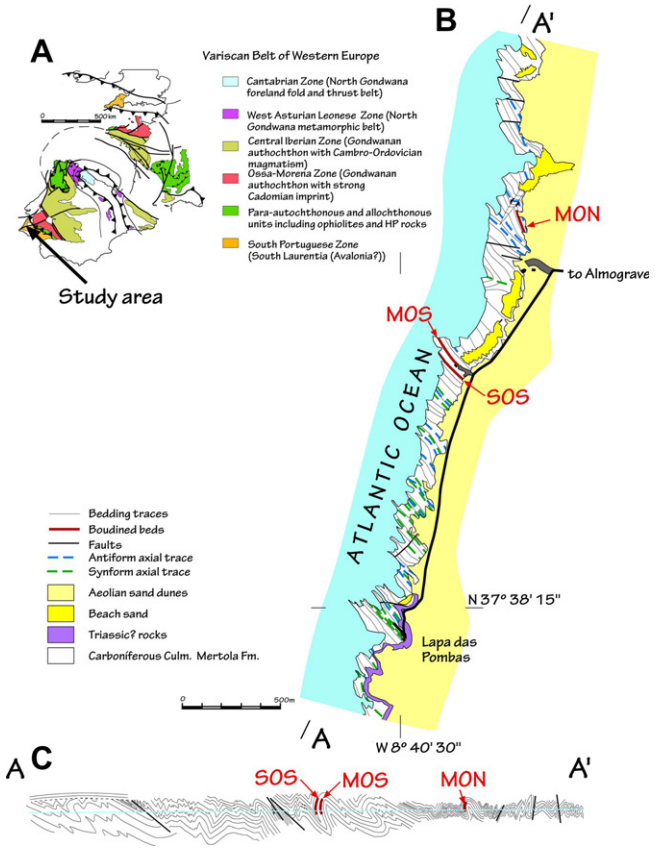

Fig. 1. Location and geology of the study area in the Variscan belt of Iberia. (A) Location of the study area and geologic sketch map of the West Europena Variscan belt indicating the position of the South Portuguese Zone and its relation to other major paleogeographic units. Grey lines are boundaries of tectonometamorphic units. Black lines with triangles are major thrusts. (B) Geologic map of the coastal exposures surrounding Almograve and location of the studied outcrops depicting chocolate-tablet boudins. (C) SSW–NNE downplunge cross-section of the study area and location of the main outcrops with chocolate-tablet boudins.

Apart from collecting and analyzing a set of structural observations, we analyzed the deformation microstructures and fluid inclusions to constrain the deformation mechanisms and temperature. Based on these new data, we present a model that explains chocolate-tablet boudinage to be the result of progressive orogenic shortening with an almost constant orientation for the main shortening direction, whereas the directions of the greatest and intermediate strain axes interchanged twice, creating the two perpendicular sets of boudin necks.

2. Methods

Field investigations were conducted along a N–S trending section to determine the overall structure and to characterize the geometrical parameters of boudins (Fig. 1). Apart from planar fabrics like bedding and cleavage planes, we measured the orientation of fold axes and crenulations. Moreover, we determined boudin thickness, boudin width, and neck width in both vertical and horizontal sections along the studied profile as well as the crosscutting relationships between the two sets of quartz veins in the boudin necks. Thin sections of boudins and neck domains were made to investigate the type of veins inside the neck domains and the deformation microstructures to help constrain the thermal history of the rocks.

Four samples of slates were investigated by X-ray powder diffractometry to determine illite crystallinity. Samples were crushed using an agate mortar or grinder and then dispersed in diluted formic acid. After multiple washings, the rock powder was treated with Na-polyphosphate to prevent coagulation. The clay mineral fractions (<2 μm) were extracted using a centrifuge machine and were evaporated onto cristal mounts, obtaining a preferred orientation of the phyllosilicates that yielded about 10 g/cm^2 of clay. This separation minimized the influence of detrital micas. From each sample several X-ray analyses were conducted to determine variations of illite crystallinity.

For X-ray diffractometry measurements a PANALYTICAL PW 3040/60 X'Pert System using a PW 3050/60 goniometer, a fine-structure copper tube and X'CELERATOR detector system PW 3015/20 were used. The illite crystallinity values are detected by full width of half measurements of the intensity of the 10 Å illite base peak maximum. Using international CIS-standards by Warr and Rice (1994), the IC values were calibrated to Kübler indices (Kübler et al., 1979), that are sensitive to detect very low-grade regional metamorphic temperature conditions between 200 °C (0,42 Δ2Θ) and 300 °C (0,25 Δ2Θ).

Fluid inclusions microthermometry was performed on doubly polished thin sections using a Linkam THM 600/S/Geo heating-freezing stage coupled to a TMS 94 temperature controller with an error of ±1 °C. The stage is mounted on an Olympus microscope with a 100× objective. The heating and cooling stage was calibrated using synthetic fluid inclusion calibration standard: CO_2 and H_2O from ©Bubbles Incorporation. The isochors were calculated using the program PVTX v2.1 from ©Linkam Instrumental.

3. Results

3.1. Structural geometries

Deformation of quartzites and slates in the studied region was polyphase. The first deformation (D_1) produced SW-vergent folds with low plunging axes (Figs. 1 and 2). The deformation formed an axial-plane cleavage in mostly of the fine-grained lithologies and

a widely spaced cleavage in the quartzites. The second deformation (D_2) involved folding around subvertical axes (Fig. 3). Because of D_2, the strike of bedding (S_0) and S_1-cleavage planes vary considerably along the studied section. This variation explains why the folds in the central part of the study area are south vergent (Fig. 2b), whereas in the northern and southern part they are SW-vergent (Fig. 2a, c). The steep axis D_2 folds are probably related to dextral transcurrent movements (Marques et al., 2010). D_1-folds are slightly asymmetric, open to tight, with thickened hinges and thinned limbs, particularly if they dip steeply to subvertical. This layer thickness change is interpreted to result from flattening strain due to amplification of the D_1-folds.

Chocolate-tablet boudins are present only in steep forelimbs of asymmetric tight D_1-folds (Fig. 1), although single sets of linear boudins with necks normal to the fold axis may occur in gentle to moderately dipping layers outside of the studied section (see also Marques et al., 2010). The boudins have a "torn" morphology (sensu Goscombe et al., 2003), because they occur either as barrel or as bow-tie vein boudins. This geometry holds for both horizontal and vertical sections (Fig. 4b,d). Vein-filled fractures are largely restricted to the neck domains and contain fibrous quartz. The quartz veins are horizontal and parallel to the fold axis, or subvertical and normal to the fold axis. In most cases, the subhorizontal veins postdate the subvertical veins, although a small number of subhorizontal veins are older (Figs. 4a,c and 5) (Marques et al., 2010; Reber et al., 2010).

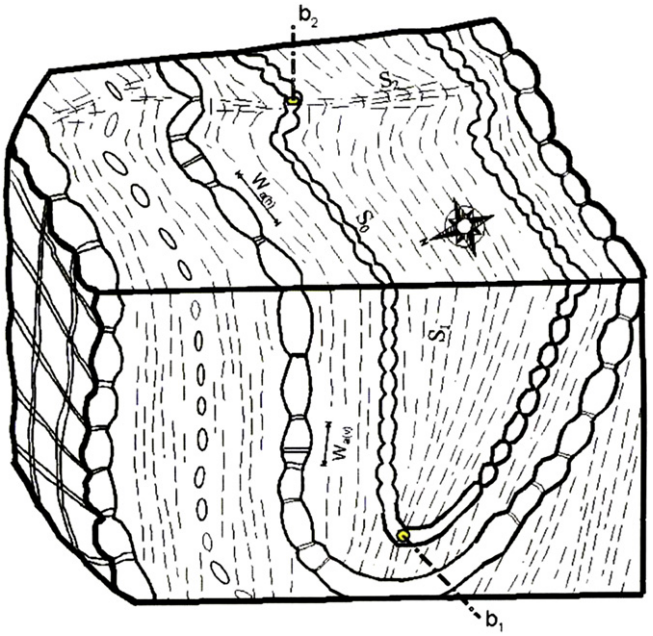

Fig. 3. Schematic drawing of chocolate-tablet boudins in quartzite layers in the steep limbs of D_1-folds with minor D_2 folds and locally developed S_2 cleavage. Long side of block could be ca. 5 m.

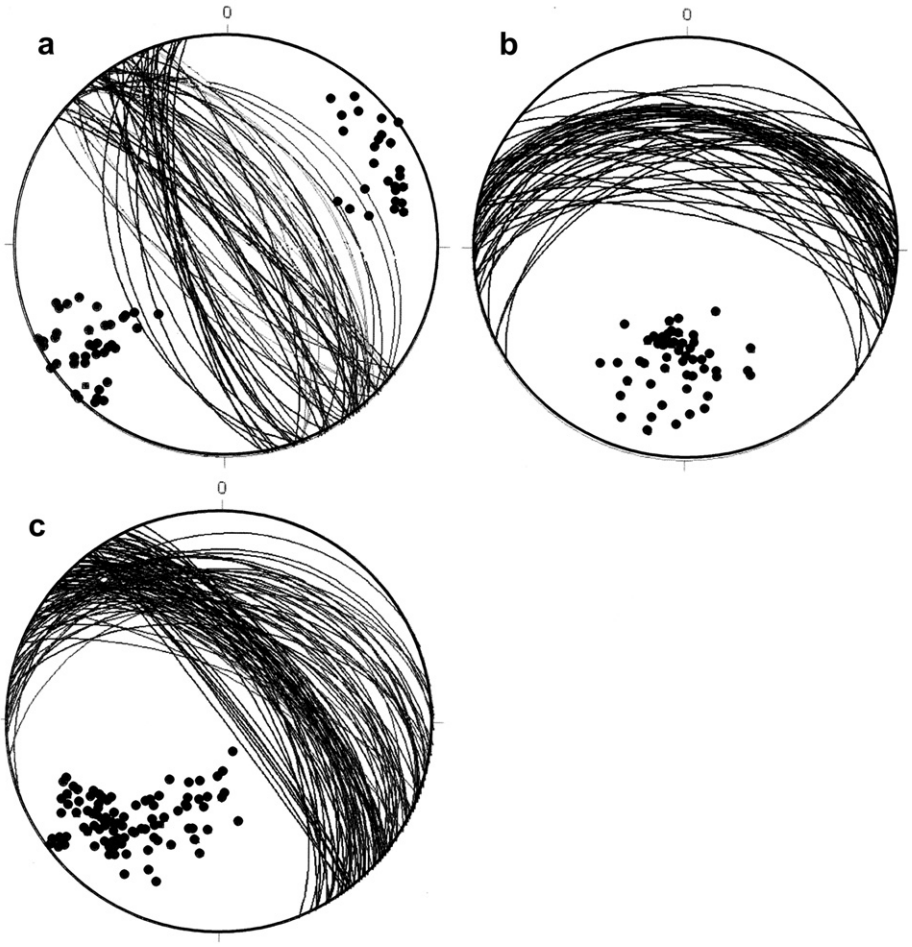

Fig. 2. Bedding orientations of shale and quartzite layers along the studied cross-section shown in Fig. 1C. (a) N part, (b) central part, (c) S part. Lower-hemisphere equal-area projection.

When considering the relationship between boudin width (W_a) and layer thickness (H_f), the number of data from horizontal sections (132) is greater than from vertical sections (43), because it is easier to sample along the horizontal than the vertical. The increase in boudin width with layer thickness is approximately linear in horizontal sections (Fig. 6):

$$W_a = 16 + 2 * H_f \quad (3)$$

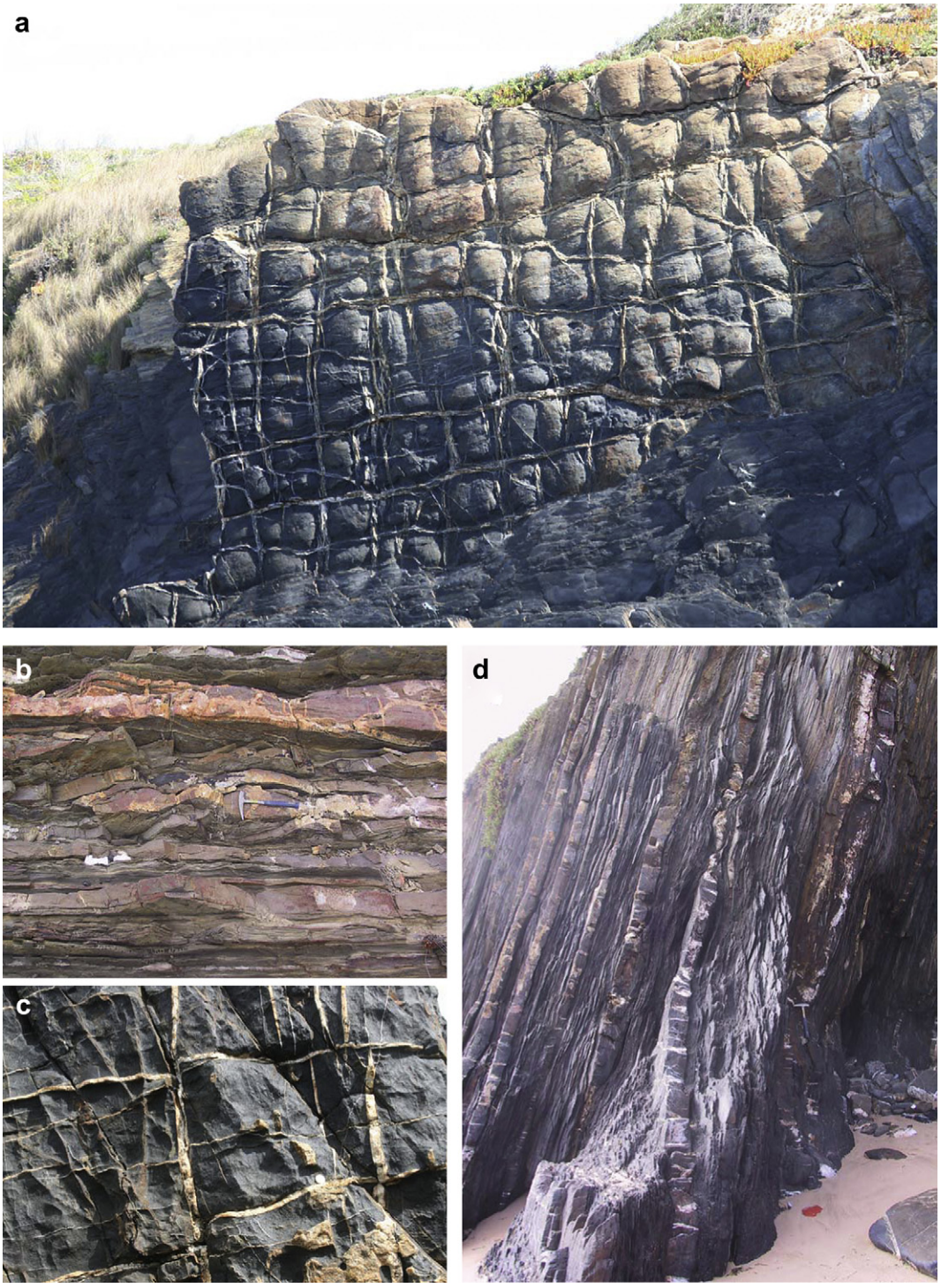

Fig. 4. Examples of chocolate-tablet structures in interbedded Carboniferous shales and quartzites. (a) View perpendicular to subvertical bedding. Boudin necks are largely decorated by quartz veins. Note that most subhorizontal necks and quartz veins are mostly younger than subvertical necks with quartz veins, because they transect them. Width of figure is ca. 8 m. (b) Horizontal section showing pinch-and-swell structures that are part of chocolate-tablet boudin morphology (hammer with length of 30 cm for scale). (c) Crosscutting relationships of quartz veins exposed on subvertical bedding plane. Note that the subvertical vein in the center-left part of the photograph is younger than the horizontal veins because it offsets them (hammer with length of 30 cm for scale). (d) Vertical section showing distinctive boudin and pinch-and-swell morphologies. Length of hammer is 30 cm.

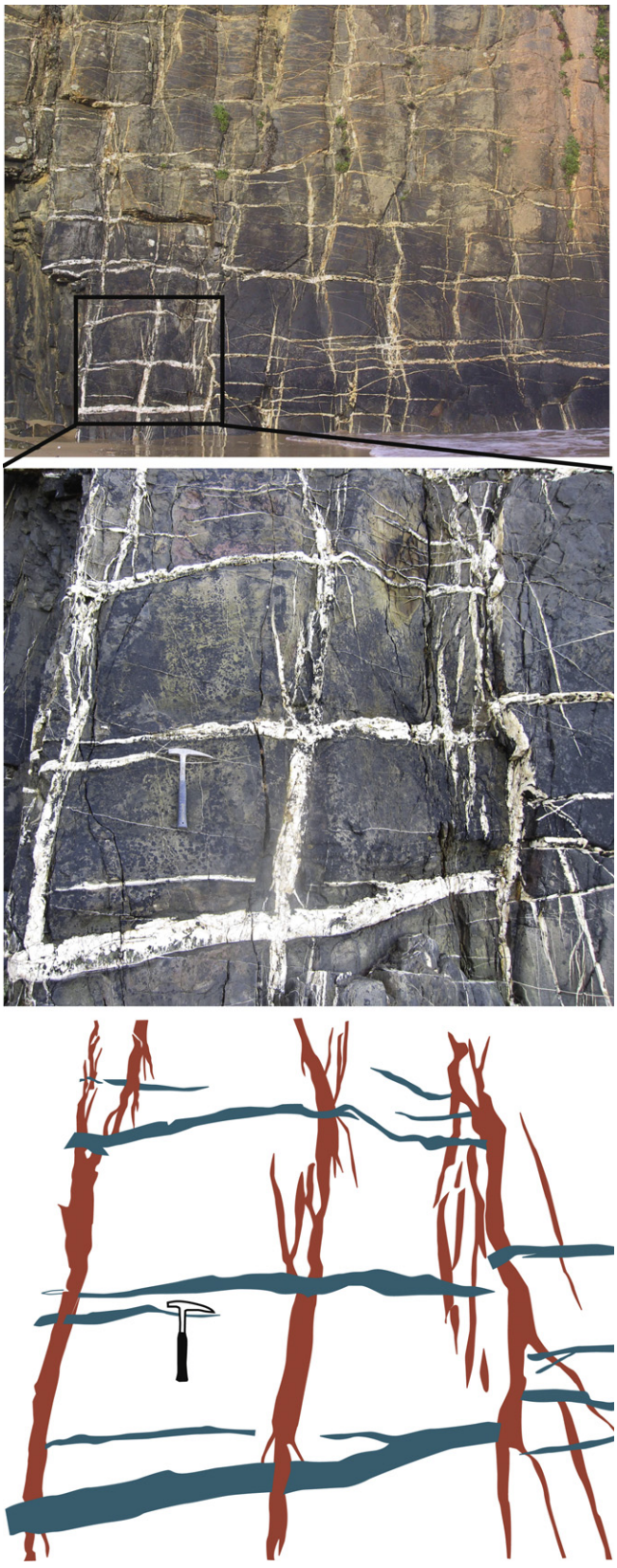

Fig. 5. Picture of outcrop labeled MOS in Fig. 1. The observed surface corresponds to the bottom of a slightly overturned bed. Detailed inset of the oucrop and sketch with the observed crosscutting relationships between the axis perpendicular veins (subvertical) and the axis parallel veins (subhorizontal). Most but not all subhorizontal veins are younger because they transect the vertical veins. Length of hammer is 30 cm.

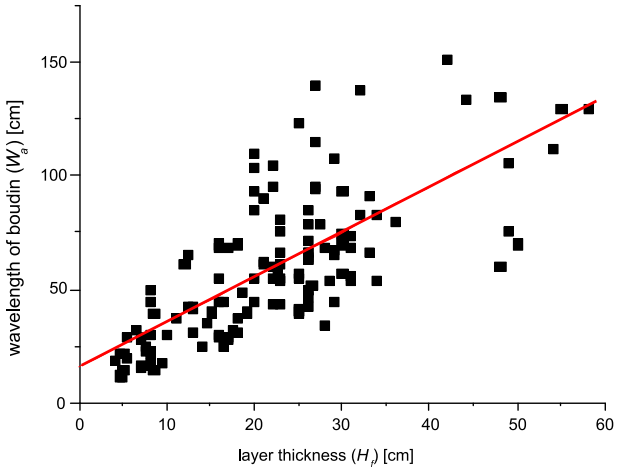

Fig. 6. Wavelength (width) of boudins (W_a) *vs.* finite layer thickness (H_f) for horizontal sections of chocolate-tablet boudins. For further explanation see text.

where the dimensions of W_a and H_f are in cm. The correlation coefficient is $R = 0.7$. The aspect ratio, W_d, for the boudins is:

$$W_d = W_a/H_f \tag{4}$$

Inserting values for W_a and H_f into Equation (4), results in W_d values of 2.9 ± 1.2 for horizontal sections, and 3.0 ± 1.4 for vertical sections.

3.2. Boudin-related microfabric

The boudins developed in beds composed of impure, fine-grained, moderately sorted quartzites where bedding is well

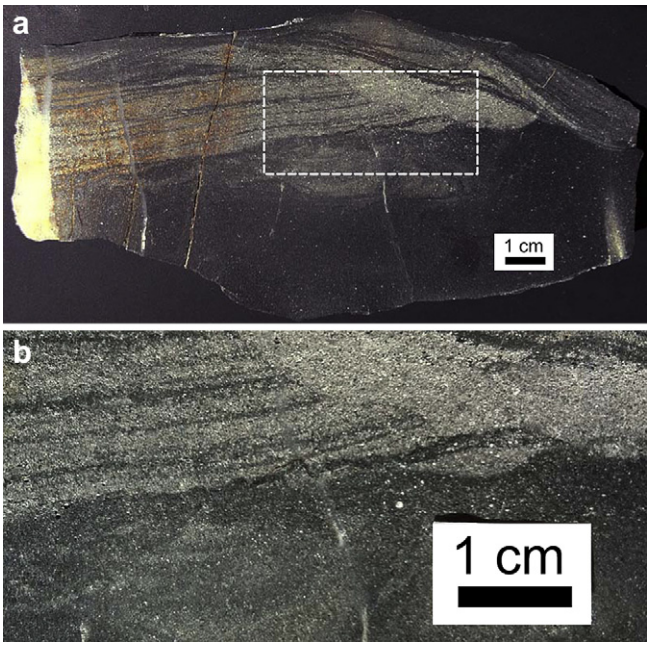

Fig. 7. (a) Photograph of quartzite boudin showing convolute bedding in the lower dark part and discordant contacts in the light material. Apart from small quartz veins inside the boudin, a wide quartz vein is present in a neck domain at the left side of the picture. White frame indicates the outline of detailed picture shown in (b). The dark lobate thin layer in the central part of (b) is a stylolite which also cuts through a small quartz vein.

preserved (Fig. 7a). In the slates most of the S_1-cleavage planes result from pressure solution as is indicated by dark seams of enriched heavy minerals and other insoluble phases (Fig. 8a). In the quartzite boudins, the S1-cleavage planes are widely spaced or absent. Evidence for solution-precipitation creep in the quartzite boudins is also present in form of pitted quartz grains (Fig. 8b), stylolites (Figs. 7b and 8c,d), and quartz fibers in strain shadows of quartz grains (Fig. 8e). In a few samples, the matrix consists locally of calcite replacing quartz grains margins. Quartz grain sizes vary from 0.01 to 0.50 mm. The mostly moderately rounded, monocrystalline quartz grains show serrated grain boundaries, undulatory extinction, deformation lamellae, and kink bands (Fig. 8f). Accessory detrital minerals in the quartzites are feldspar, chlorite, epidote, titanite, white mica and opaque phases. Feldspar grains are altered to secondary minerals such as sericite or zoisite.

Small veins are present inside boudins and show a first-phase mineralization of an opaque phase, probably hematite, and a second phase of blocky quartz grains. The blocky quartz grains occur in the vein centers and show several wall-rock-parallel inclusion trails consisting of the minerals present in the opaque phase. Other small veins inside the boudins are filled only with syntaxial quartz fibers. Discrete small-displacement faults are decorated by opaque phases and show quartz fibers inside *en echelon* dilational jogs.

3.3. Microfabric of the neck domains

Almost all neck domains, both vertical and horizontal, show centimeter-scale quartz veins that are up to 4 cm wide. Most quartz veins in the *vertical necks* have at least two generations of

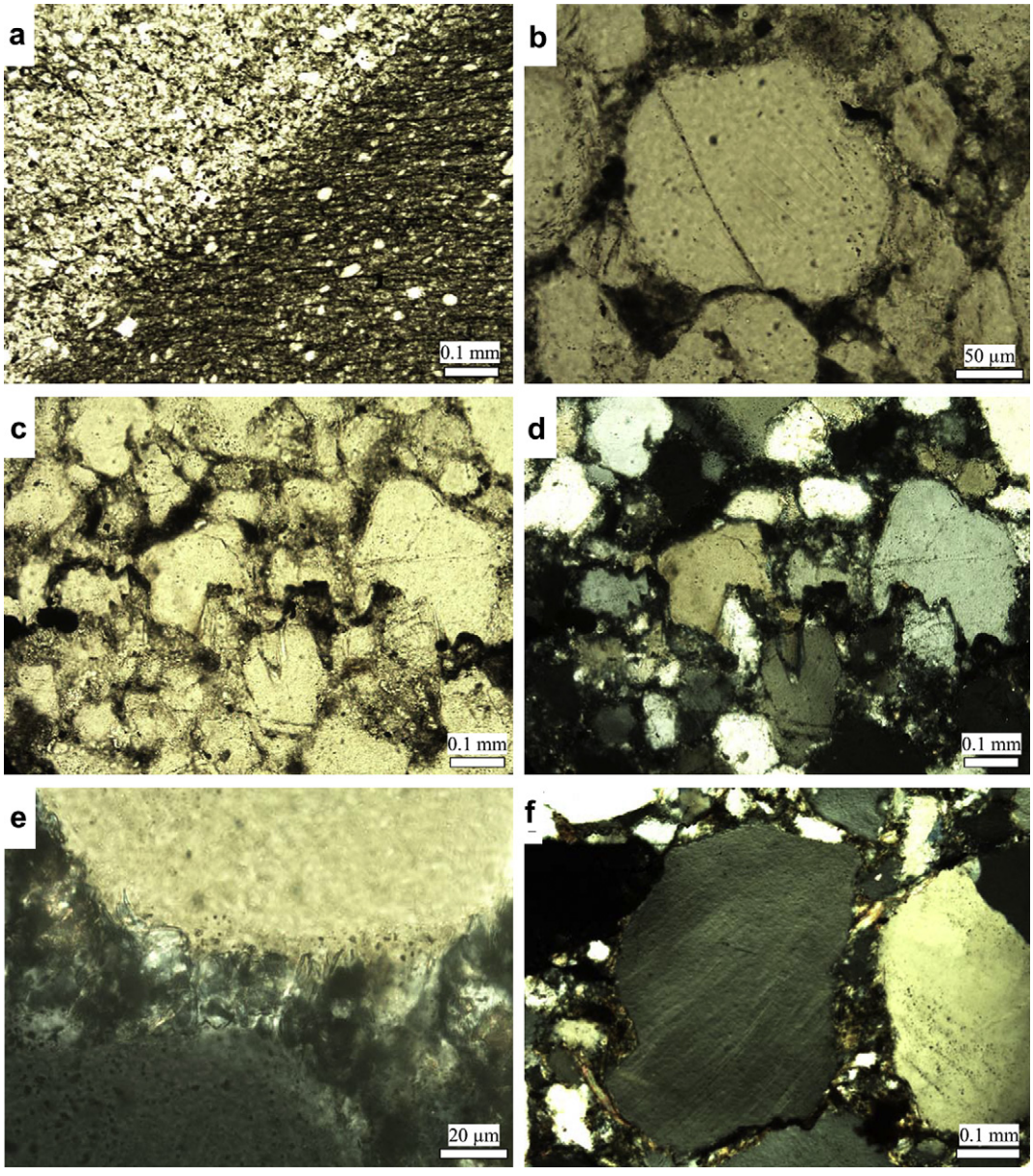

Fig. 8. Photomicrographs of quartzite boudins. (a) Bedding contact between pelitic (dark) and psammitic layer (light). The closely spaced S_1-cleavage in the pelitic domain (horizontal in picture) is characterized by enrichment of insoluble phases. The same S_1-cleavage is refracted and widely spaced in the psammitic part. Parallel polarizers. (b) Large pitted quartz grain results from indentation of a smaller quartz grain. The contact between both grains is decorated by dark insoluble phases. Parallel polarizers. (c) Stylolite transecting quartz grains. Parallel polarizers. (d) Same picture like in (c) but with crossed polarizers. (e) Quartz fibers in strain shadow between two quartz grains. Crossed polarizers. (f) Numerous kink bands affecting a quartz grain. Note also the serrated boundary of the quartz grain. Crossed polarizers.

symmetrically arranged fibers (Fig. 9c). The first generation of fibers developed along vein walls and consists of small fibers that are mostly straight and 0.2–0.5 mm wide. Syntaxial growth of these fibers is indicated by optical continuity between the fibers and the grains of the wall-rock. The second generation of quartz fibers occupies the center of the vein and consists of fibers showing optical continuity with the first generation of fibers. Moreover, most second-generation fibers form a crystallographically continuous link from one side to the other and thus can be interpreted as 'stretched crystal fibers' (*sensu* Ramsay and Huber, 1983). The stretched crystal fibers are wider than the first generation of fibers, ranging from 0.4 to 2.0 mm. The boudin necks also contain narrower veins mineralized with only one generation of narrow fibers (Fig. 9a). These fibers are morphologically similar to those formed during the first generation of the wider veins.

Most quartz veins of the *horizontal necks* also show two generations of fibers (Fig. 9d). The first generation consists of syntaxial fibers, which are 0.1–0.4 mm wide, occurring at the vein margins. The younger generation in the central part of the veins consisting of stretched crystal fibers that are, however, larger than those of the vertical necks. The width of the stretched crystal fibers varies between 0.5 and 3.0 mm. Some second-generation fibers consist of blocky minerals.

All fibers show fluid inclusions which are either homogeneously distributed within the crystals or occur as fluid inclusion trails, many of which are aligned subparallel to the vein walls (Fig. 10c). Weak to moderate crystal-plastic deformation of the quartz fibers of both vertical and horizontal veins is indicated by undulatory extinction, deformation lamellae, kink bands, and serrated grain boundaries (Fig. 9c,d and 10a,b,d). Subgrains are restricted to high-strain domains (Fig. 10a,b).

3.4. Constraints on deformation temperature

X-ray diffraction analyses of four slate samples show that the whole-rock and fine fraction (<2 μm) of the slates mainly consist of illite and chlorite together with minor amounts of kaolinite (Table 1). Illite dominates in the clay fractions. Illite is dioctaedral,

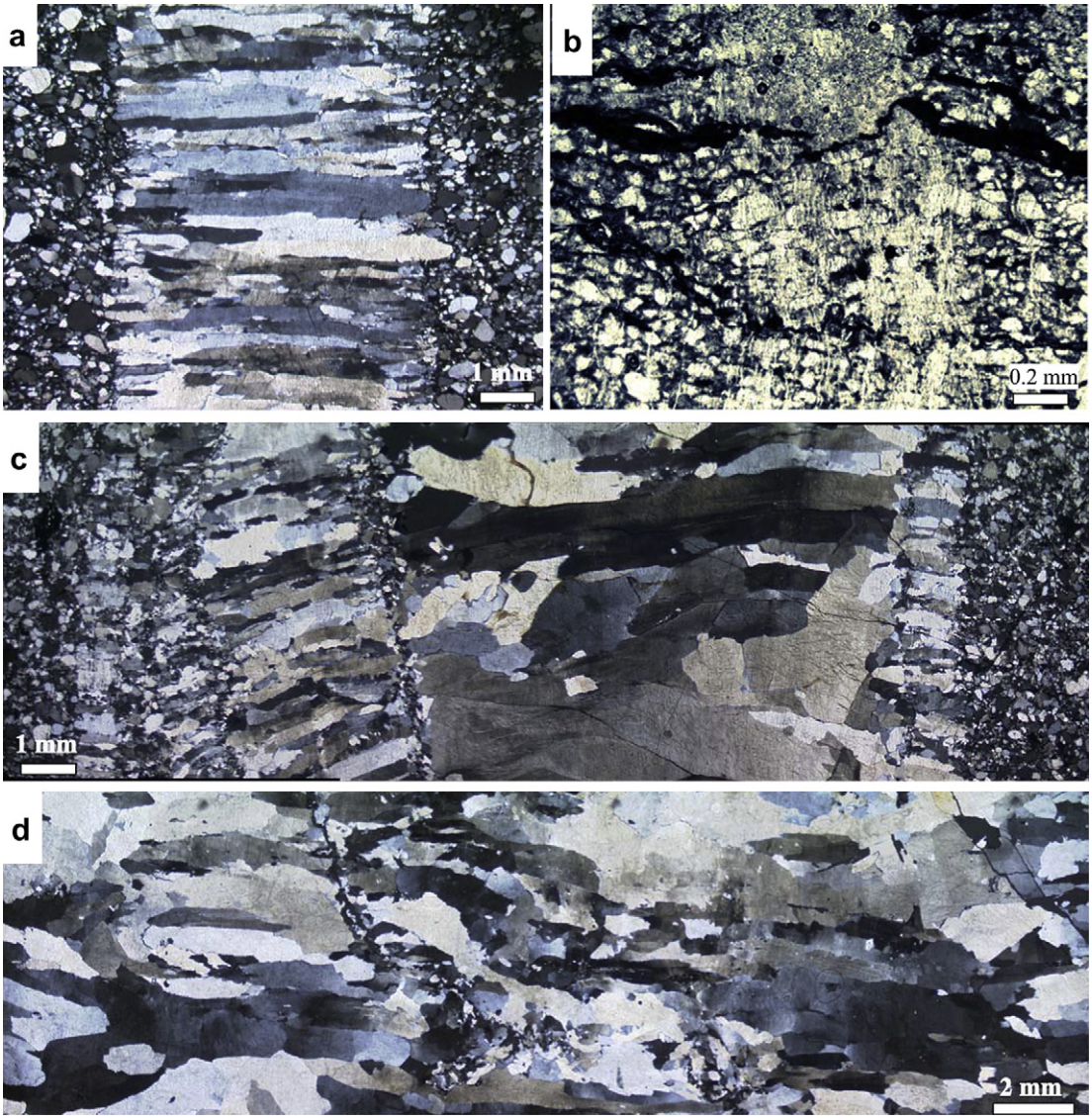

Fig. 9. Photomicrographs of quartz veins from the neck domains. All pictures produced under crossed polarizers, apart from (b). (a) Quartz fibers in vein of vertical neck resulting from syntaxial growth from one wall to the other (stretched crystal fibers). (b) Fine-grained impure quartzite is cut by a small vertical quartz vein which shows numerous wall-rock-parallel inclusion trails. Both quartzite and vein quartz are affected by two stylolites. (c) Two phases of fiber growth in quartz vein of a vertical neck. (d) Large irregular blocky quartz crystals inside a vein of a horizontal neck domain. For further explanation, see text.

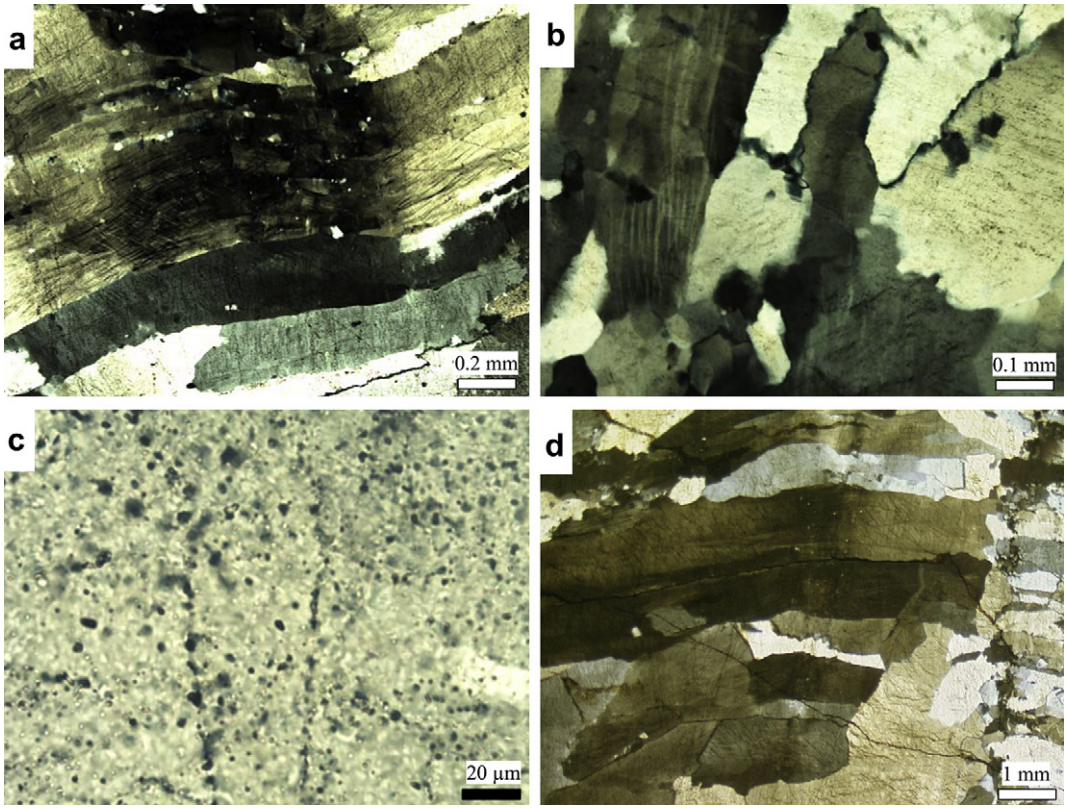

Fig. 10. Microstructures and fluid inclusions in vein quartz of neck domains; all pictures produced with crossed polarizers. (a) Bent quartz fiber of vertical vein shows undulatory extinction, kink bands, subgrains, and serrated grain boundaries. (b) Kink bands, serrated grain boundaries, and subgrains in deformed vertical vein of a neck domain. (c) Fluid inclusions in vertical quartz vein are either homogeneously distributed or arranged subparallel to the vein wall. (d) Deformed quartz fiber of a vertical vein showing undulatory extinction, serrated grain boundaries and partly subgrains.

Al rich and consists of about 75% 2M and 25% 1M polytypes. The CIS calculated illite crytallinity values range from 0.37 to 0.43 Δ2Θ with a mean of 0.39, suggesting uppermost diagenetic to very low-grade metamorphic conditions and temperatures ranging between 200 °C and 250 °C (Ferreiro-Mählmann, 1994). This temperature interval is consistent with the previous characterization of illite crystallinity in the South Portuguese Zone (Abad et al., 2001).

Fluid inclusions were examined in two of crosscutting veins located in the boudin necks. The chronology of the different fluid inclusion populations is a relative to their host mineral and their overgrowth (Mullis, 1976). In both cases, the horizontal vein postdates the vertical vein. Veins are mainly composed of small quartz crystals. Samples *Mn4* and *Mn7* showed no CH_4, CO_2 or HHC gases in the fluid for primary, pseudo-secondary or both inclusion types. As none of the investigated fluid inclusions contained any observable gas component, salinity was determined from the ice melting temperature in NaCl-equivalence after Potter et al. (1978). In both samples, the fluid inclusion assemblage is a two-phase type trapped during quartz growth (Mullis, 1987).

In sample *Mn7*, the fluid inclusions from the vertical veins have a size of 4–10 μm and an estimated vapour/liquid volume ratio of 0.10, a mean (homogenization temperature) $Th_I = 180 \pm 30$ °C, and a mean (melting temperature) $T_m = 2.80 \pm 0.50$ °C corresponding to a salt density of 4.61% NaCl eqwt.

Fluid inclusions in the horizontal veins of sample *Mn7* vary in size from 4 to 10 μm. The vapor/liquid ratio is estimated at 0.10, and the mean Th_I is 220 ± 44 °C corresponding to a density of 5.27% NaCl eqwt ($T_m = -3.25 \pm 0.30$ °C).

In sample *Mn4*, the fluid inclusion size in the vertical neck varies between 3 and 10 μm and their vapor/liquid ratio is estimated at 0.10. The mean Th_I is 173 ± 20 °C, the inclusions have a density around 5.39% NaCl eqwt, with a $T_m = -3.35 \pm 0.30$ °C.

The fluid inclusions in the horizontal neck of sample *Mn4* have a size of 4–10 μm and an estimated vapor/liquid volume ratio of 0.10, a mean $Th_I = 196 \pm 22$ °C, and a mean $T_m = -3.40 \pm 0.20$ °C corresponding to a high density of 5.50% NaCl eqwt.

Therefore, the type and distribution of fluid inclusions (primary and secondary) in both types of veins is similar. Also, the fluid composition and derived formation temperature of both sets of quartz veins are the same within uncertainty. Assuming a normal geothermal gradient of 30 °C km^{-1} during vein opening, the formation temperature of the fluid inclusions are calculated at 200 ± 20 °C and 200 ± 24 °C for the vertical veins, and 230 ± 22 °C and 230 ± 44 °C for the horizontal veins (Fig. 11a–d).

Table 1
Results of X-ray diffraction analyses of the four different slates analyzed in this study.

	Illite 001 10 Å FWHM CIS Kübler	Illite Rel %	Kaolinite Rel %	Chlorite Rel %	Comment
ALMO 1	0.399	63.7	4.3	32.0	
ALMO 2	0.372	60.4	8.9	30.7	
ALMO 3	0.430	93.0	0.0	7.0	?analcime
ALMO 4	0.370	71.9	0.0	28.1	?smectite

4. Discussion

The crosscutting relationship of vertical and horizontal necks suggest that the chocolate-tablet boudins did not form during one single deformation event, but result from two-phase necking and fracturing, starting with the development of the vertical necks and

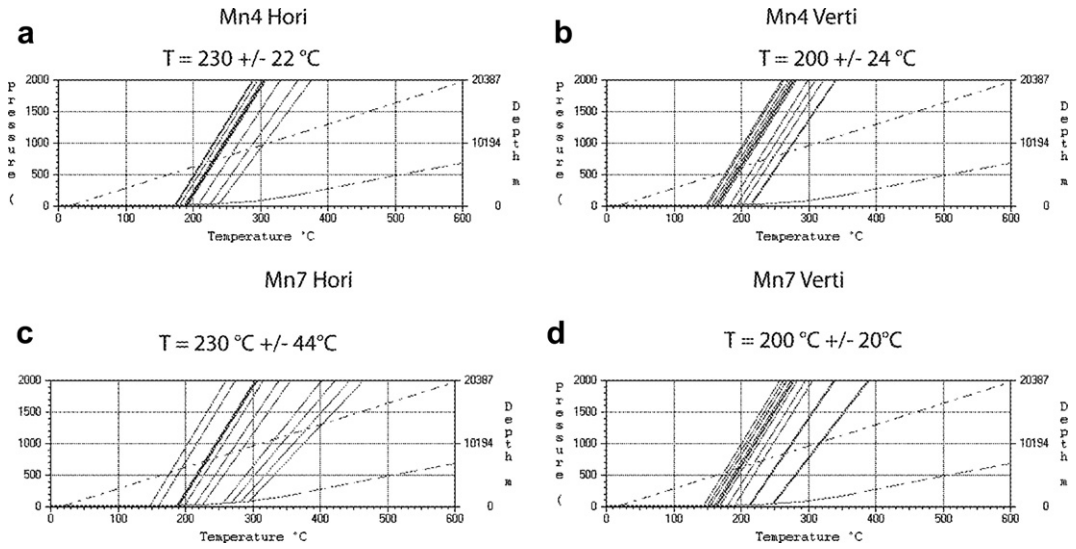

Fig. 11. Temperature estimates from fluid inclusions. (a) Horizontal neck of sample Mn4. (b) Vertical vein of sample Mn4. (c) Horizontal vein of sample Mn7. (d) Vertical vein of sample Mn7. For further explanation, see text.

veins followed by horizontal necks and veins, although some horizontal extension occurred coevally (Fig. 5; Reber et al., 2010).

At first sight, the formation of each set of necks and boudins was related to *brittle tensile failure* and resulted in torn boudins. In this particular case veining and boudinage are closely associated (see also Cervantes and Wiltschko, 2010, and references therein). Tensile fracture boudinage is controlled by the transfer of stress from the ductile matrix (slate) to the brittle quartzite layer (e.g. Ramberg, 1955; Hobbs, 1967; Lloyd et al., 1982; Narr and Suppe, 1991; Wu and Pollard, 1995; Bai et al., 2000).

The barrel geometry of the boudins suggests that brittle tensile fracture was probably not the only mechanism which contributed to the formation of the boudins. This assumption is also supported by the boudin aspect ratio, W_d, that is controlled by the rheological parameters of matrix and layer (e.g. Ramberg, 1955; Smith, 1977, 1979). The aspect ratios obtained for the two sets of boudins (2.9 ± 1.2 in horizontal sections, and 3.0 ± 1.4 in vertical sections) are in the range of ratios described from natural torn boudins in the literature (Goscombe et al., 2003). Experiments using rock analogs have shown that viscous necking or a combination of viscous necking and subsequent extension fracture results in boudin aspect ratios ranging from 3 to 12 (Schöpfer and Zulauf, 2002; Zulauf and Zulauf, 2005; Enama-Mengong and Zulauf, 2005; Zulauf et al., 2010; Zulauf et al., in press).

The similar W_d values in vertical and horizontal sections suggest that the boudinage in both directions (vertical and horizontal) occurred under similar conditions. Microthermometry based on fluid inclusions also suggest that both sets of necks and veins have formed under similar temperatures (200 ± 20 °C for the vertical veins, and 230 ± 22 °C for the horizontal veins). This temperature range reflects conditions at or slightly above the diagenesis/anchimetamorphic transition that is also indicated by the illite crystallinity data. Given the host rock and the precipitating fluid were in thermal equilibrium, the fibrous quartz of the neck domains should have developed close to the metamorphic peak. The deformation microstructures of the quartz fibers (undulatory extinction, kink bands, deformation lamellae, lobate grain boundaries and rare subgrains) indicate dislocation glide as the most important mechanism, which is compatible with the proposed temperature conditions listed above (e.g. Oncken, 1990; Zulauf et al., 2002). Evidence for pervasive operation of recovery and recrystallization of quartz that should be expected in quartz veins deformed at $T >$ ca. 270 °C (Voll, 1976; Takeshita and Hara, 1998; Nishikawa and Takeshita, 2000; Zulauf, 2001; Stipp et al., 2002), is lacking. The same applies to the quartz grains inside the boudins. We interpret the presence of stylolites, pitted quartz grains, and quartz fibers in strain shadows of quartz grains to have occurred during the fluid-assisted particulate flow (Marques et al., 2010). Recrystallization fabrics observed in sparse polycrystalline detrital quartz grains of the quartzite could be inherited from the previously deformed rocks in the provenance area.

The large number of wall-rock-parallel fluid inclusion trails inside the stretched crystal fibers suggests the veins to have formed by the 'crack-seal' mechanism (Ramsay, 1980). This means that the fibers grew sequentially by the alternately development of small openings and cementation by quartz precipitation. The precipitating fluids contributed to solution-precipitation creep, particularly in the slates (Marques et al., 2010). Solution-precipitation creep is active at low to moderate differential stress, when tension gashes may form.

From the results presented above we conclude that the chocolate-tablet structures inside the Carboniferous slates and quartzites near Almograve developed close to the local metamorphic peak during the latemost increments of the D_1 shortening phase. During D_1-folding the main shortening direction was subhorizontal and oriented perpendicular to the fold axes, while the intermediate strain axis was oriented parallel to the fold axes and the main stretching axis was subvertical (Fig. 12b). Shortening under these conditions led to southwest-verging tight to isoclinal folds with steep backlimbs to subvertical or slightly overturned forelimbs. The process by which the chocolate-tablet boudins formed is interpreted to be sequential sets of extension-related fractures that developed during one progressive deformation phase. After the limbs of the D_1-folds had attained their steep attitude, especially the forelimb, progressive shortening caused flattening of the steep limbs with the main shortening direction being still oriented subhorizontal, i.e. subvertical to bedding. The two other principal strain axes, however, switched their attitude. The intermediate strain axis was now oriented subvertical and the main stretching axis was subhorizontal, i.e. parallel to the fold axes. In this environment layer-parallel horizontal extension led to the first set of necks and

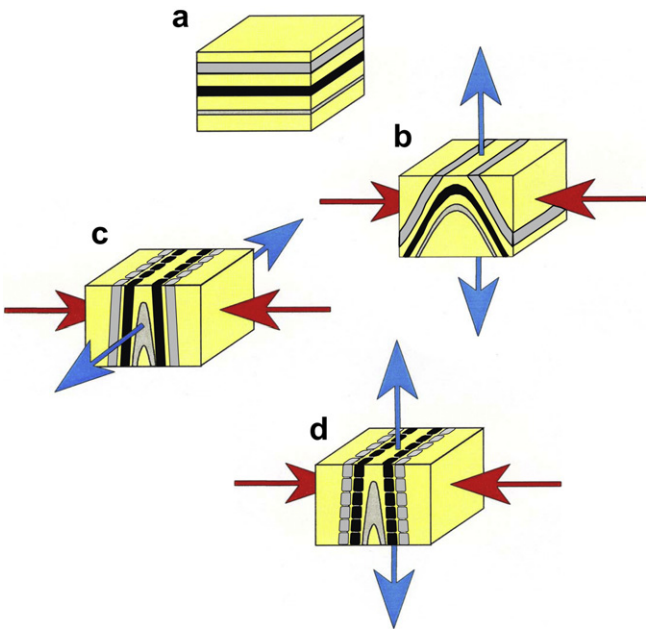

Fig. 12. Model of folding and subsequent polyphase evolution of chocolate-tablet boudins near Almograve. Red arrows show major shortening direction. Blue arrows show main stretching direction. (a) Sequence of shale and quartzite before deformation. (b) Horizontal shortening results in folding and progressive steepening of limbs. (c) Consistent shortening cannot be accommodated by further thickening but by extension parallel to the strike of bedding resulting in the first-phase of boudinage with vertical necks. (d) Extension in the steeper or overturned limb results in horizontal necks. The combination of horizontal and vertical necks results in chocolate-tablet boudins. (For interpretation of the references to colour in this figure legend, the reader is referred to the web version of this article).

extension fractures, both of which are subvertical (Fig. 12c). Subsequently, the orientation of the main stretching axis and the intermediate strain axes were interchanged once more. The stretching axis rotated again into vertical, and the intermediate strain axis was again horizontal and parallel to the fold axes. As a result the second set of (horizontal) necks and extension fractures formed in the steeper or slightly overturned forelimbs of some folds (Fig. 12d). Similar conclusions have been drawn from detailed analyses of the progressive changes in the stress-strain fields in folds developed under similar conditions elsewhere (e.g. Pfiffner, 1990; Gutiérrez-Alonso and Gross, 1999).

It has to be emphasized that the orientation of the main shortening direction did not significantly change during D_1-folding and during subsequent stages of necking and boudinage. This assumption is compatible with results of Marques et al. (2002, 2010), who concluded that in the southwest Portugal domain the stress field did not appreciably change its orientation during Variscan folding. Our conclusions are further in line with the results of Reber et al. (2010), who performed numerical simulations investigating the evolution of stress orientations during folding to test whether and how these two successive sets of fractures were related to folding. 3D simulations demonstrate that the principal stretching axis rotates with and within bedding, in the fold limb, from a fold axis parallel to a fold axis orthogonal direction.

A similar formation of chocolate-tablet boudinage with fibrous crystal growth like that described in the present study has been described from Leytron, Valais, Switzerland, where the deformation history was found to be a succession of plane-strain increments with the shortening direction perpendicular to the boudinaged sheet and the extension direction showing a progressive change in orientation within the sheet (Casey et al., 1983).

5. Conclusions

The following conclusions can be drawn from the present study:

- Formation of chocolate-tablet boudins in Carboniferous pelitic and psammitic layers near Almograve is intimately related to folding in the foreland fold and thrust belt of the external Variscides.
- Folds and boudins developed during progressive shortening of the mechanically stratified layers with the main shortening direction being constant in horizontal orientation. A two-fold switch of the intermediate and greatest principal strain axes led to two sets of extension fractures (boudin necks) that are perpendicular to each other, resulting in chocolate-tablet boudins.
- From the shape and aspect ratio of the boudins, we conclude that the boudin width was not controlled by extension fracture but by ductile necking that was accommodated by solution-precipitation creep. Ductile necking led to a reduction in layer thickness and thus a drop in strength of the pinched domains that made the latter prone for subsequent extension fracture.
- Chocolate-tablet boudins, separated by two sets of orthogonal necks, cannot develop inside a mechanically homogeneous competent layer in a flattening type of bulk deformation, but require at least two phases of extension under nearly plane-strain conditions. This conclusion is in line with results of analog modeling, which show that a single phase of pure flattening results in tablet boudins which have a polygonal shape in plan-view (Ghosh, 1988; Zulauf et al., 2010, in press).

Acknowledgments

The studies were supported by grants of Deutsche Forschungsgemeinschaft (DFG, grant Zu 73/21-1), DAAD (314-Al-e-dr) and MEC-Ministerio de Educación Ciencia in the frame of the exchange program ‘Acciones Integradas Hispano Alemanas 2007’. G.G.-A. Also acknowledges financial support from Research Project ODRE II (CGL2009-1367) from the Spanish Ministry of Science and Innovation. We are grateful to E. Gottwald for preparing the thin sections and to E. Schaub for preparing the XRD samples. We thank William M. Dunne, Daniel Koehn and David V. Wiltschko for providing thoughtful reviews that improved the manuscript.

References

Abad, I., Mata, M.P., Nieto, F., Velilla, N., 2001. The phyllosilicates in diagenetic metamorphic rocks of the south Portuguese zone, Southwestern Portugal. Can. Mineral. 39, 1571–1589.
Albertz, M., Paterson, S., 2002. Three-dimensional pure shear during transpression: the effect of cretaceous plutonism on regional strain fields in the Sierra Nevada batholith, California. GSA Abstracts with Programs, 37th Annual Meeting (March 25–27, 2002).
Bai, T., Pollard, D.D., Gao, H., 2000. Explanation for fracture spacing in layered materials. Nature 403, 753–756.
Casey, M., Dietrich, D., Ramsay, J.G., 1983. Methods of determining deformation history for chocolate tablet boudinage with fibrous crystals. Tectonophysics 92, 211–239.
Cervantes, P., Wiltschko, D.V., 2010. Tip to midpoint observations of syntectonic veins, Quachita orogen, Arkansas: Trading space for time. J. Struct. Geol. 32, 1085–1100.
Coe, K., 1959. Boudinage structures in West Cork, Ireland. Geol. Mag. 96, 192–200.
Crespo-Blanc, A., 1995. Interference pattern of extensional fault systems: a case study of the Miocene rifting of the Alhoran basement (North of Sierra Nevada, Betic Chain). J. Struct. Geol. 17, 1559–1569.
Enama-Mengong, M., Zulauf, G., 2005. Coeval folding and boudinage under bulk plain strain, with the axis of no change perpendicular to the layering. Int. J. Earth Sci. 95, 178–188.
Ferreiro Mählmann, R., 1994. Zur Bestimmung von Diagenesehöhe und beginnender Metamorphose - Temperaturgeschichte und Tektogenese des

Austroalpins und Südpenninikums in Voralberg und Mittelbünden. Frankfurter geowissenschaftliche Arbeiten, C 14, 1–498.
Fyson, W.K., 1962. Tectonic structures in the Devonian rocks near Plymouth, Devon. Geol. Mag. 99, 208–226.
Ghosh, S.K., 1988. Theory of chocolate tablet boudinage. J. Struct. Geol. 10, 541–553.
Goscombe, B.D., Passchier, C.W., Hand, M., 2003. Boudinage classification: end-member boudin types and modified boudin structures. J. Struct. Geol. 26, 739–763.
Gutiérrez-Alonso, G., Gross, M.R., 1999. Structures and mechanisms associated with development of a fold in the Cantabrian zone thrust belt, NW Spain. J. Struct. Geol. 21, 653–670.
Hobbs, D.W., 1967. The formation of tension joints in sedimentary rocks: an explanation. Geol. Mag. 104, 550–556.
Kenis, I., Sintubin, M., Muchez, Ph., Burke, E.A.J., 2002. The "boudinage" question in the High-Ardenne Slate Belt (Belgium): a combined structural and fluid-inclusion approach. Tectonophysics 348, 93–110.
Kübler, B., Pittion, J.-L., Héroux, Y., Charollais, J., Weidmann, M., 1979. Sur le pouvoir réflecteur de la vitrinite dans quelques roches du Jura, de la Molasse et des Nappes préalpines, helvétiques et penniques. Ecolcgae geologica Helveticae 72, 343–373.
Lohest, M., 1909. De l'origine des veines et des géodes des terrains primaries de Belgique. Troisième note. Annls. Soc. Géol. Belg. 36, 275–282. Bull for 1908–1909.
Lloyd, G.E., Ferguson, C.C., Reading, K., 1982. A stress-transfer model for the development of extension fracture boudinage. J. Struct. Geol. 4, 355–372.
Marques, F.O., Mateus, A., Tassinari, C., 2002. The Late-Variscan fault network in centralnorthern Portugal (NW Iberia): a reevaluation. Tectonophysics 359, 255–270.
Marques, F.O., Burg, J.-P., Lechmann, S.M., Schmalholz, S.M., 2010. Fluid-assisted particulate flow of turbidites at very low temperature: a key to tight folding in a submarine Variscan foreland basin of SW Europe. Tectonics 29 (2). doi:10.1029/2008TC002439.
Mullis, J., 1976. Das Wachstumsmilieu der Quarzkristalle im Val d'Illiez (Wallis, Schweiz). Schweizerische Mineralogische und Petrologische Mitteilungen 56, 219–268.
Mullis, J., 1987. Fluid inclusion studies during very low-grade metamorphism. In: Frey, M. (Ed.), Low Temperature Metamorphism. Blackie, Glasgow, pp. 162–199.
Narr, W., Suppe, J., 1991. Joint spacing in sedimentary rocks. J. Struct. Geol. 13, 1037–1048.
Nishikawa, O., Takeshita, T., 2000. Progressive lattice misorientation and micro-structural development in quartz veins deformed under subgreenschist conditions. J. Struct. Geol. 22, 259–276.
Oliveira, J.T., 1990. South Portuguese Zone: stratigraphy and synsedimentary tectonism. In: Dallmeyer, R.D., Martínez García, E. (Eds.), Pre-Mesozoic Geology of Iberia. Springer, Berlin, Germany, pp. 334–347.
Oncken, O., 1990. Aspects of the structural and paleogeothermal evolution of the Rhenish Massif. Annales de la Société Géologieque de Belgique 113, 139–159.
Onezime, J., Charvet, J., Faure, M., Bourdier, J.L., Chauvet, A., 2003. A new geodynamic interpretation for the South Portuguese Zone (SW Iberia) and the Iberian pyrite belt genesis. Tectonics 22.
Onezime, J., Charvet, J., Faure, M., Chauvet, A., Panis, D., 2002. Structural evolution of the southernmost segment of the West European Variscides: the south Portuguese zone (SW Iberia). J. Struct. Geol. 24, 451–468.
Ormand, C.J., Czeck, D., 2003. Structure and kinematics of the baraboo syncline: a three-dimensional analysis. GSA Abstracts with Programs, 35/6, p. 341.
Pfiffner, O.A., Ramsay, J.G., 1982. Constraints on geological strain rates: arguments from finite strain states of naturally deformed rocks. J. Geophys. Res. 87, 311–321.
Pfiffner, O.A., 1990. Kinematics and intrabed-strain in mesoscopically folded limestone layers: examples from the Jura and the Helvetic Zone of the Alps. Eclogae Geol. Helv 83/3, 585–602.
Potter II, R.W., Clynne, M.A., Brown, D.L., 1978. Freezing point depression of aqueous sodium solutions. Econ. Geol. 73, 284–285.
Quesada, C., 1991. Geological constraints on the Palaeozoic tectonic evolution of the tectonostratigraphic terranes in the Iberian Massif. Tectonophysics 185, 225–245.
Ramberg, H., 1955. Natural and experimental boudinage and pinch-and-swell structures. J. Geol. 63, 512–526.
Ramsay, J.G., 1967. Folding and Fracturing of Rocks. McGraw-Hill Book Co., New York, 568 pp.
Ramsay, J.G., 1980. The crack-seal mechanism of rock deformation. Nature 284, 135–139.
Ramsay, J.G., Huber, M.I., 1983. The Techniques of Modern Structural Geology. In: Strain Analysis, vol. 1. Academic Press, 307 pp.
Reber, J.E., Schmalholz, S.M., Burg, J.-P., 2010. Stress orientation and fracturing during three-dimensional buckling: numerical simulation and application to chocolate-tablet structures in folded turbidites, SW Portugal. Tectonophysics 493, 187–195.
Schöpfer, M.P.J., Zulauf, G., 2002. Strain dependent rheology and the memory of plasticine. Tectonophysics 354, 85–99.
Schwerdtner, W.M., Clark, A.R., 1967. Structural analysis of Mokka Fiord and south Fiord domes, Axel Heiberg Island, Canadian Arctic. Can. J. Earth Sci. 4, 1229–1245.
Silva, J.B., Oliveira, J.T., Ribeiro, A., 1990. The south Portuguese zone. Structural outline. In: Dallmeyer, R.D., Martínez-García, E. (Eds.), Pre-Mesozoic Geology of Iberia. Springer-Verlag, Berlin, pp. 334–362.
Smith, R.B., 1977. Formation of folds, boudinage, and mullions in non-Newtonian materials. Geol. Soc. Am. Bull. 88, 312–320.
Smith, R.B., 1979. The folding of a strongly non-Newtonian layer. Am. J. Sci. 279, 272–287.
Soriano, C., Casas, J.M., 2002. Variscan tectonics in the Iberian pyrite belt, south Portuguese zone. Int. J. Earth Sci. 91, 882–896.
Stipp, M., Stünitz, H., Heilbronner, R., Schmid, S.M., 2002. The eastern Tonale fault zone: a "natural laboratory" for crystal plastic deformation of quartz over a temperature range from 250 to 700–°C. J. Struct. Geol. 24, 1861–1884. doi:10.1016/S0191-8141 (02)00035-4.
Takeshita, T., Hara, I., 1998. c-axis fabrics and microstructures in a recrystallized quartz vein deformed under fluid-rich greenchist conditions. J. Struct. Geol. 20, 417–431.
Tricart, P., Schwartz, S., Sue, C., Lardeaux, J.-M., 2004. Evidence of synextension tilting and doming during final exhumation from analysis of multistage faults (Queyras Schistes lustre's, Western Alps). J. Struct. Geol. 26, 1633–1645.
Voll, G., 1976. Recrystallization of quartz, biotite, feldspars from Erstfeld to the Leventina Nappe, Swiss Alps, and its geological significance. Schweiz. Mineral. Petrogr. Mitt. 56, 641–647.
Warr, L.N., Rice, A.H.N., 1994. Interlaboratory standardization and calibration of day mineral crystallinity and crystallite size data. J. Metamorph. Geol. 12, 141–152.
Wegmann, C.E., 1932. Note sur le boudinage. Bull. Soc. Géol. France 2, 477–491.
Weijermars, R., 1997. Principles of Rock Mechanics. Alboran Science Publishing, 359 pp.
Witkowski, C.M., Crespi, J.M., 2002. Absolute finite strains from reconstructions of fractured pyritized graptolites and volume change in the Taconic slate belt, eastern New York. GSA Abstracts with Programs, 37th Annual Meeting (March 25–27, 2002).
Wu, H., Pollard, D.D., 1995. An experimental study of the relationship between joint spacing and layer thickness. J. Struct. Geol. 17, 887–905.
Zulauf, G., 2001. Structural style, deformation mechanisms and paleodifferential stress along an exposed crustal section: constraints on the rheology of quartzofeldspathic rocks at supra- and infrastructural levels (Bohemian Massif). Tectonophysics 332, 211–237. doi:10.1016/S0040-1951(00)00258-4.
Zulauf, J., 2004. Analog modellierung von Falten und Boudins in Raum und Zeit. Erlanger Geologische Abhandlungen 135, 115.
Zulauf, J., Zulauf, G., 2005. Coeval folding and boudinage in four dimensions. J. Struct. Geol. 27, 1061–1068.
Zulauf, G., Kowalczyk, G., Petschick, R., Schwanz, S., Krahl, J., 2002. The tectono-metamorphic evolution of high-pressure low-temperature metamorphic rocks of eastern Crete, Greece: constraints from microfabrics, strain, illite crystallinity and paleostress. J. Struct. Geol. 24, 1805–1828.
Zulauf, G., Zulauf, J., Hastreiter, P., Tomandl, B., 2003. A deformation apparatus for three-dimensional coaxial deformation and its application to rheologically stratified analogue material. J. Struct. Geol. 25, 469–480.
Zulauf, J., Zulauf, G., Kraus, R., Gutiérrez-Alonso, G., Zanella, F., 2010. The origin of tablet boudinage: results from experiments using power-law rock analogs. Tectonophysics. doi:10.1016/j.tecto.2011.07.013.
Zulauf, G., Zulauf, J., Hammer, J., Zanella, F. Tablet boudinage of an anhydrite layer in rock-salt matrix: Results from thermomechanical experiments. J. Struct. Geol., in press.